IEEE Access
Multidisciplinary | Rapid Review | Open Access Journal

Received January 19, 2021, accepted January 25, 2021, date of publication February 2, 2021, date of current version February 10, 2021.

Digital Object Identifier 10.1109/ACCESS.2021.3056485

S-Shaped Metasurface-Based Wideband Circularly Polarized Patch Antenna for C-Band Applications

NATHAPAT SUPREEYATITIKUL[1], TITIPONG LERTWIRIYAPRAPA[2], (Senior Member, IEEE), AND CHUWONG PHONGCHAROENPANICH[1], (Member, IEEE)

[1]School of Engineering, King Mongkut's Institute of Technology Ladkrabang, Bangkok 10520, Thailand
[2]Research Center of Innovation Digital and Electromagnetic Technology, Department of Teacher Training in Electrical Engineering, Faculty of Technical Education, King Mongkut's University of Technology North Bangkok, Bangkok 10800, Thailand

Corresponding author: Chuwong Phongcharoenpanich (chuwong.ph@kmitl.ac.th)

This work was supported by the King Mongkut's University of Technology North Bangkok under Grant KMUTNB-64-KNOW-29.

ABSTRACT This research proposed an S-shaped metasurface (MTS)-based wideband circularly polarized (CP) patch antenna for C-band uplink frequency spectrum. The proposed MTS-based CP patch antenna was of low profile and fabricated on three substrate layers: upper, middle, and lower. The upper substrate contained 4 × 4 periodic S-shaped MTS elements, the middle substrate functioned as ground plane with a rectangular-shaped slot at the center, and the lower substrate contained a coplanar waveguide with microstrip and ground. The S-shaped MTS elements converted linearly polarized (LP) into CP wave. Simulations were performed, and an antenna prototype was fabricated and experiments carried out. The measured impedance bandwidth and axial ratio bandwidth (ARBW) at the center frequency of 5.9 GHz were 43.22% (4.05 – 6.6 GHz) and 22% (5.3 – 6.6 GHz), respectively, rendering the proposed antenna suitable for satellite communication applications. The proposed antenna achieved the maximum gain of 6.16 dBic at 5.6 GHz. The novelty of this research lies in the use of S-shaped MTS elements to efficiently convert LP into CP wave and achieve wider ARBW for the C-band uplink spectrum.

INDEX TERMS C-band, circularly polarized antenna, low-profile, metasurface, wideband.

I. INTRODUCTION

Modern low-profile wideband circularly polarized (CP) antennas are utilized in a wide range of wireless applications, including satellite communication, global navigation satellite systems (GNSS), radio frequency identification (RFID), wireless power harvesting, and wireless sensors [1]–[4]. Compact CP antennas were used in mobile devices, RFID handheld readers, WLAN access points, and handheld satellite terminals [5]–[8]. In [9], CP antennas are also used to overcome multipath interferences.

The advances in wireless communication devices necessitate the development of new low-profile CP antennas with wider circular polarization bandwidth, i.e., impedance bandwidth (IBW) and axial ratio bandwidth (ARBW). To enhance CP bandwidth, several techniques were adopted in the design and development of broadband CP antennas, including a square slot antenna with an L-shaped feed [10], a ring slot with a hybrid coupler [11], stacked patches [12], coplanar parasitic patches [13], and dielectric resonators [14]. However, these CP antennas suffer from design complexity, bulkiness, and low CP bandwidth performance.

To address the drawbacks, metasurface-based structures have been adopted in the design of more recent wideband CP antennas with enhanced CP bandwidth. Metasurface (MTS) structures are used to convert linear polarization (LP) to circular polarization (CP) wave. The MTS structures are two-dimensional (2D) equivalents of metamaterials which are fashioned from artificial materials and composed of periodically-arranged small elements. The advantages of MTS-based CP antenna include ease of fabrication, low profile, and high CP bandwidth performance.

Due to the compact size and inexpensiveness, patch antennas are typically deployed in the design and development of MTS-based wideband CP antennas. In [15], a circular-ring-slot single-fed microstrip patch antenna with

The associate editor coordinating the review of this manuscript and approving it for publication was Raghvendra Kumar Kumar Chaudhary.

7×7 rectangular-ring MTS units functioning as artificial magnetic conductor reflector for C-band spectrum could achieve an IBW of 36% (3.22 – 4.63 GHz) and 3-dB ARBW of 28.3% (3.62 – 4.75 GHz). A CP single-fed corner-truncated square Fabry-Perot patch antenna with simple MTS structure for C-band spectrum achieved an IBW of 31.7% (5.23 – 7.20 GHz) and 3-dB ARBW of 13.7% (5.45 – 6.25 GHz) [16]. In [17], a crossed dipole CP antenna with 6×6 rectangular MTS structure achieved an IBW of 31.6% (2 – 2.75 GHz) and 3-dB ARBW of 23.2% (2.1 – 2.65 GHz). In [18], a novel sandwiched anisotropic metasurface consisting of an elliptical patch as the radiator above the metasurface and a superstrate as partially reflecting surface for C-band spectrum could achieve an IBW of 35.29% (3.08 – 4.40 GHz) and 3-dB ARBW of 24.69% (3.55 – 4.56 GHz).

The MTS-based CP antennas [16]–[18] require a cavity resonant condition (i.e., air gaps between substrates) to realize wide CP bandwidth [19], resulting in antenna bulkiness due to the gaps. To tackle the bulkiness, compact MTS-based CP antennas were proposed to efficiently improve the IBW, ARBW, and radiation performance [20]–[21]. In [22], a lattice MTS-based linearly polarized slot-coupled antenna was proposed to convert LP to CP wave based on two resonance modes: TM_{10} and TM_{20} modes (TM denotes transverse magnetic wave). The lattice MTS-based antenna could achieve broad IBW (16%, 3.67 – 4.29 GHz) and 3-dB ARBW (10%, 3.9 – 4.27 GHz).

Specifically, this research proposes a low-profile S-shaped MTS-based wideband CP patch antenna for the C-band uplink frequency spectrum. The S-shaped MTS functions as the superstrate of the proposed patch antenna because the MTS (i.e., superstrate) [23] is of an ultrathin two-dimension artificial layer, consisting of periodically arranged S-shaped MTS elements. The MTS-based CP antenna was fabricated on three substrate layers: upper, middle, and lower. The upper substrate contained 4×4 periodic S-shaped MTS elements to convert LP into CP wave, the middle substrate functioned as the ground plane with a rectangular slot at the center, and the lower substrate contained a coplanar waveguide with microstrip and ground. Simulations were performed by using CST Studio Suite, and an antenna prototype was fabricated and experiments carried out.

The organization of this research is as follows: Section I is the introduction. Section II describes the configuration of the S-shaped MTS-based wideband CP patch antenna, and Section III details the proposed antenna evolution and MTS operation. Section IV deals with the parametric study and simulation. Section V discusses the experimental results. The concluding remarks are provided in Section VI.

II. ANTENNA CONFIGURATION

Figure 1 illustrates the geometry of the S-shaped MTS-based wideband CP patch antenna for the C-band uplink frequency spectrum (5.925 – 6.425 GHz). The proposed MTS-based CP antenna was fabricated on three layers of FR-4 substrate:

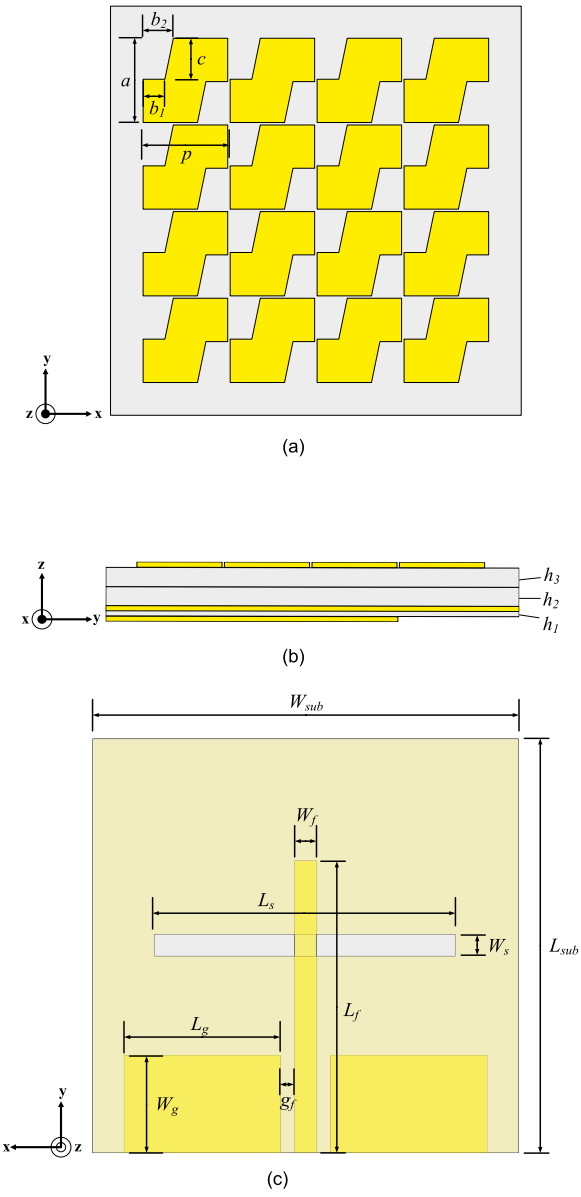

FIGURE 1. Geometry of the S-shaped metasurface-based wideband CP patch antenna: (a) front view, (b) side view, (c) rear view.

upper, middle, and lower, without air gap between substrates. The thickness of the upper (h_1), middle (h_2), and lower (h_3) substrates were 0.8 mm, 1.6 mm, and 1.6 mm, respectively. The dielectric constant (ε_r) and loss tangent ($tan\ \delta$) of the substrates were 4.3 and 0.025, and the substrate dimension was 34×34 mm ($W_{sub} \times L_{sub}$).

The upper substrate contained 4×4 periodic S-shaped MTS elements. The vertical length (a) of one S-shaped MTS element was 7 mm, and the length of the MTS element including voids (p) was 7.4 mm. The void between two S-shaped MTS elements was 0.4 mm. The S-shaped MTS element evolved from square-shaped MTS element, resulting in identical vertical and horizontal lengths of the S-shaped element. The middle substrate contained a copper plate functioning as the ground plane with a rectangular-shaped

TABLE 1. Parameters and optimal dimensions of the proposed S-shaped MTS wideband CP patch antenna.

Parameters	L_{sub}	W_{sub}	L_g	W_g	L_f	W_f	g_f	L_s	W_s	p	a	c	b_1	b_2	h_1	h_2	h_3
Value (mm)	34	34	12.5	8	24	1.8	1.1	25	2	7.4	7	3.5	1.8	2.5	0.8	1.6	1.6

slot at the center. The dimensions of the ground plane and rectangular-shaped slot were 34 × 34 mm ($W_{sub} \times L_{sub}$) and 2 × 25 mm ($W_s \times L_s$).

The lower substrate consisted of a coplanar waveguide (CPW) with a microstrip feed line and ground, fed by an SMA connector. The dimensions of the microstrip feed line and ground were 1.8 × 24 mm ($W_f \times L_f$) and 8 × 12.5 mm ($W_g \times L_g$). The distance between the feed line and the ground (g_f) was 1.1 mm. The overall dimension of the S-shaped MTS-based wideband CP patch antenna was 34 × 34 × 4 mm (0.485 λ_0× 0.485 λ_0× 0.057 λ_0, where λ_0 is the free-space wavelength corresponding to the lowest operating frequency achievable by the proposed S-shaped MTS-based CP antenna at 4.25 GHz). Table 1 tabulates the parameters and optimal dimensions of the proposed S-shaped MTS wideband CP patch antenna. Simulations were carried out using CST Studio Suite.

III. ANTENNA EVOLUTION AND MTS OPERATION

A. EVOLUTION OF S-SHAPED MTS-BASED CP PATCH ANTENNA

Figure 2 shows the evolution stages of the S-shaped MTS-based wideband CP patch antenna, consisting of three stages: first stage (Antenna I), second stage (Antenna II), and final stage (Antenna III). Antenna I was comprised of a rectangular-shaped slot at the center of the ground plane (the middle substrate) and CPW on the lower substrate (Figure 2(a)). In Antenna II, the upper substrate containing 4 × 4 symmetric square-shaped MTS was integrated with Antenna I (Figure 2(b)). To realize circular polarization, the square-shaped MTS elements were truncated for S-shaped MTS elements (Antenna III), as shown in Figure 2(c). Specifically, Antenna III was comprised of 4 × 4 periodic S-shaped MTS elements on the upper substrate, a rectangular slot at the center of the ground plane on the middle substrate, and CPW on the lower substrate.

Figure 3 illustrates the simulated IBW ($|S_{11}| \leq -10$ dB) and ARBW (AR ≤ 3 dB) of Antennas I, II, and III. In Figure 3(a), Antenna I achieved the first resonance ($|S_{11}| \leq -10$ dB) between 4.3 – 5.15 GHz and the second resonance between 6.4 – 6.75 GHz. The IBW of Antenna I however failed to fully cover the C-band uplink frequency spectrum (5.925 – 6.425 GHz). The IBW of Antenna II (5.25 – 6.8 GHz) covered the C-band uplink spectrum, but the AR was greater than 3 dB (AR > 3 dB). Antenna III achieved two resonance frequencies at 5.1 GHz and 6.2 GHz, with IBW (4.3 – 6.5 GHz) covering the C-band uplink spectrum.

Figure 3(b) shows the simulated ARBW (AR ≤ 3 dB) of Antenna III, with ARBW covering 5.5 – 6.8 GHz. Since the AR of Antennas I and II were excessively larger than 3 dB (approximately 40 and 31 dB for Antennas I and II), their simulated ARBW were a linear polarization.

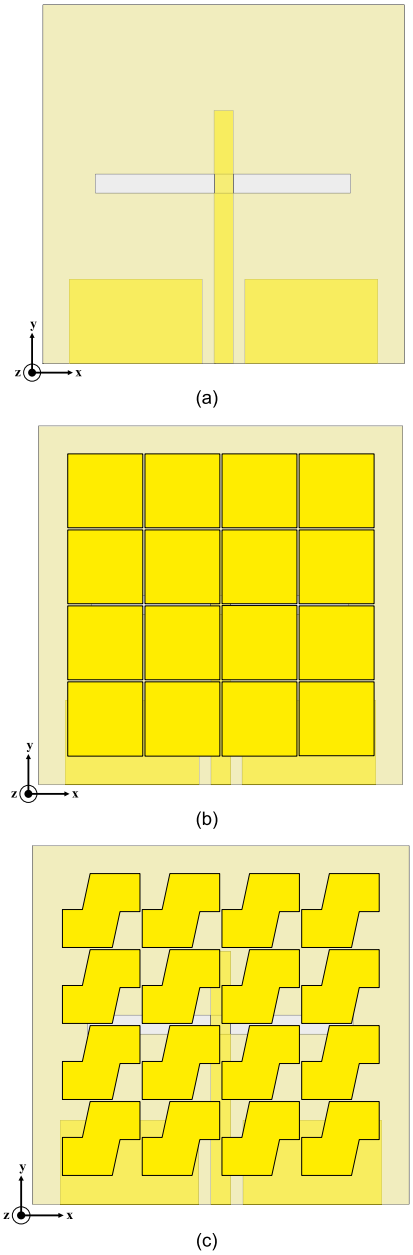

FIGURE 2. Evolution of the S-shaped MTS-based wideband CP patch antenna: (a) Antenna I, (b) Antenna II, (c) Antenna III.

B. MTS OPERATION

The coupling between the rectangular-shaped slot (on the middle substrate) and the S-shaped MTS (on the upper substrate) was characterized by two resonance modes: TM_{10}

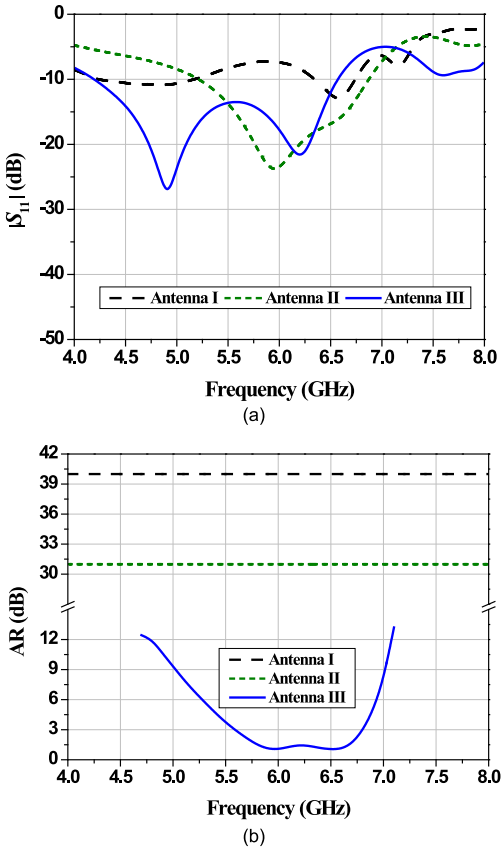

FIGURE 3. Simulated results of Antennas I, II, and III: (a) impedance bandwidth, (b) axial ratio bandwidth.

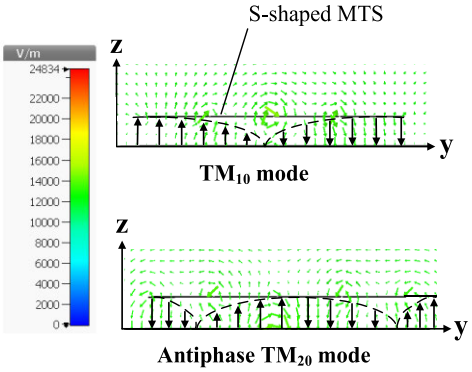

FIGURE 4. Diagrams of TM_{10} and TM_{20} modes at 5.9 and 6.5 GHz.

and TM_{20} modes (Figure 4). The cavity model was used to determine the resonance modes of the S-shaped MTS-based CP patch antenna [24]. The resonance frequencies of TM_{10} and TM_{20} modes can be determined by equations (1) and (2), respectively [25].

$$\beta_0 p N_x + 2\beta_{eff}\Delta L = \pi \quad (1)$$

$$\beta_0 p N_x/2 + 2\beta_{eff}\Delta L = \pi \quad (2)$$

where β_0 is the propagation constant of an S-shaped MTS element, N_x is the number of MTS elements in the x direction ($N_x = 4$), β_{eff} is the propagation constant in the effective extended region (i.e., the void between any pair of S-shaped elements) in the x direction, and ΔL is the distance between any pair of S-shaped elements. β_{eff} can be calculated by using equations (3) – (6) [26, 27].

$$\beta_{eff} = k_0\sqrt{\varepsilon_{reff}} = \frac{2\pi f}{c}\sqrt{\varepsilon_{reff}} \quad (3)$$

$$\frac{\Delta L}{h} = 0.412\frac{(\varepsilon_{reff}+0.3)(W_p/h+0.262)}{(\varepsilon_{reff}-0.258)(W_p/h+0.813)} \quad (4)$$

$$\varepsilon_{reff} = \frac{\varepsilon_r+1}{2} + \frac{\varepsilon_r-1}{2}\left(1+12\frac{h}{W_p}\right)^{-1/2} \quad (5)$$

$$W_p = N_y p - \left(\frac{p-a}{2}\right) \quad (6)$$

where k_0 is the wave number in free space, f is the operating frequency, and c is the free-space velocity of light, ε_{reff} is the effective dielectric constant, ε_r is the relative permittivity of substrate, h is the height of the middle and upper substrates ($h_2 + h_3$), and W_p is the effective width of an S-shaped MTS (i.e., the width of the MTS element and voids on either side), and N_y is the number of MTS elements in the y direction ($N_y = 4$).

Using equations (1) and (2), the phase shift ($\beta_0 p/\pi$) of an S-shaped MTS element in TM_{10} and TM_{20} modes were 0.195 and 0.378, corresponding to the resonance frequencies of 5.97 GHz and 6.48 GHz, as shown in Figure 5. The resulting resonance frequencies were consistent with the electrical field of the two resonance modes at 5.9 and 6.5 GHz (Figure 4).

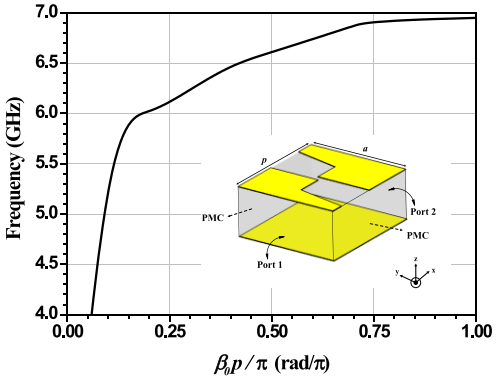

FIGURE 5. Dispersion diagram of S-shaped MTS element.

The circular polarization of the S-shaped MTS-based wideband CP patch antenna was characterized by the phase difference between the far-field boresight (+z) direction electric fields of two orthogonal components (E_x and E_y) and the corresponding magnitude ratio [28].

Figure 6 shows the phase difference between electric fields of two orthogonal components ($\angle E_y$ - $\angle E_x$) and magnitude ratio ($|E_y|/|E_x|$). The phase difference was approximately ±90° in the frequency range of 5.3 – 7.6 GHz, as shown in Figure 6(a), and the magnitude ratio was ±3 dB in the 4.1 – 7.9 GHz frequency range (Figure 6(b)).

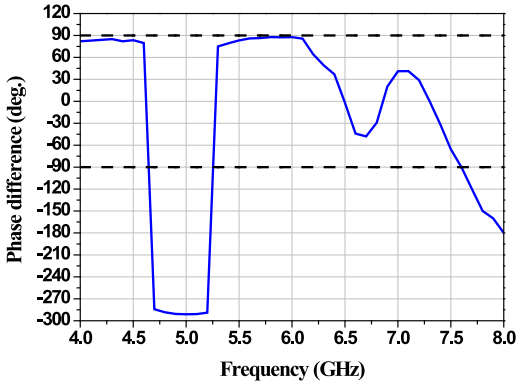

(a)

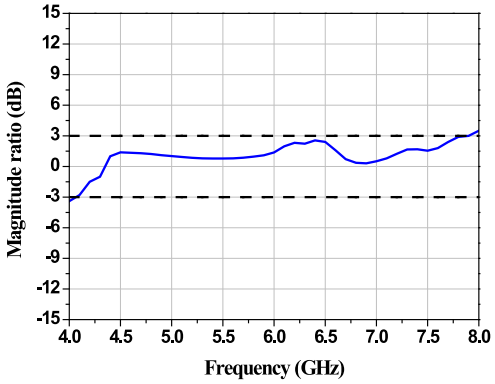

(b)

FIGURE 6. Simulated results of the proposed S-shaped MTS-based CP patch antenna: (a) phase difference, (b) magnitude ratio.

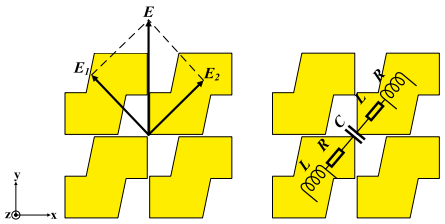

(a) (b)

FIGURE 7. Cluster of S-shaped MTS elements: (a) four-element cluster, (b) equivalent circuit model.

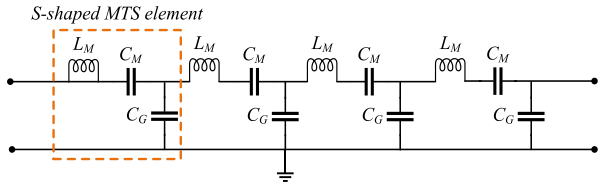

(a)

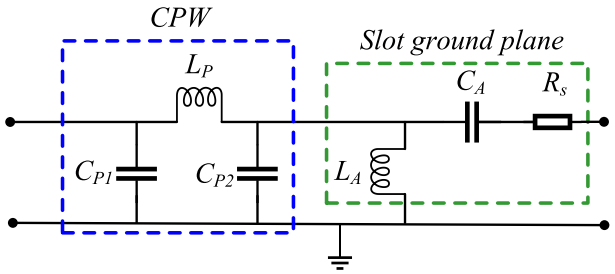

(b)

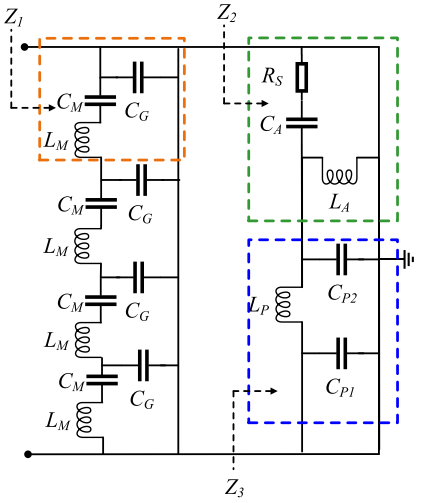

(c)

FIGURE 8. Equivalent circuit diagrams: (a) 4 × 4 S-shaped MTS, (b) CPW with slot ground plane, (c) the proposed S-shaped MTS-based CP patch antenna.

Figure 7(a) illustrates a cluster of four S-shaped MTS elements of the proposed MTS-based CP patch antenna. In the operation, the coupling between the rectangular-shaped slot on the middle substrate and the CPW on the lower substrate generated LP wave in the direction of electric field (E) along the Y-axis and, upon contact with the four-element cluster, diverged into two orthogonal electric fields (E_1 and E_2). Figure 7(b) shows the equivalent circuit model of four-element cluster whose impedance (Z_i) can be calculated by using (7) [29].

$$Z_i = R_i + j\omega L_i + 1/j\omega C_i \tag{7}$$

where R_i, L_i, and C_i are the resistance, inductance, and capacitance of two diagonally adjacent MTS elements where $i = 1, 2$; j is the imaginary inductance and capacitance; and ω is the angular frequency. To realize circular polarization, the impedance of two orthogonal electric fields (Z_1 and Z_2) must be identical ($|Z_1| = |Z_2|$) and ($\angle Z_1 - \angle Z_2$) = $\pm 90°$.

Figures 8(a)-(c) show the equivalent circuit diagrams of 4 × 4 S-shaped MTS elements on the upper substrate; CPW with slot ground plane on the lower substrate; and the proposed S-shaped MTS-based CP patch antenna, respectively. In Figure 8(a), the equivalent circuit diagram of an S-shaped MTS element [30] consisted of inductor (L_M), series capacitor (C_M), and parallel capacitor (C_G), representing the S-shaped MTS element, a void between any pair of S-shaped MTS elements, and the coupling between the S-shaped MTS element and the slot ground plane, respectively.

In Figure 8(b), the equivalent circuit diagram of CPW [31], [32] consisted of inductor (L_P), parallel capacitor (C_{P1}), and parallel capacitor (C_{P2}), representing the microstrip feed line, the gap between the microstrip feed line and the ground, and the coupling between CPW and the slot ground plane. Specifically, the equivalent circuit diagram of the slot ground plane [33] consisted of inductor (L_A), capacitor (C_A), and resistor (R_S), representing the copper plate, rectangular-shaped slot, and resistance of the ground plane.

In Figure 8(c), the equivalent circuit diagram of the proposed S-shaped MTS-based CP patch antenna consisted of the parallelly-connected equivalent circuits in Figures 8(a) and (b). The impedance of S-shaped MTS element (Z_1), slot ground plane (Z_2), and CPW (Z_3) can be calculated by equations (8) – (10), respectively.

$$Z_1 = (L_M + C_M)||C_G = \frac{j(1-\omega^2 C_G L_M)}{\omega(\omega^2 C_M C_G L_M - C_M - C_G)} \quad (8)$$

$$Z_2 = (R_s + C_A)||L_A = \frac{j\omega R_s L_A + L_A/C_A}{R_s + (1-\omega^2 L_A C_A)/j\omega C_A} \quad (9)$$

$$Z_3 = L_P||C_{P1}||C_{P2} = \frac{-j\,(L_P/\omega C_{P1} C_{P2})}{j\omega L_P + 1/j\omega\,(1C_{P1} + 1/C_{P2})} \quad (10)$$

The components (R, L, C) of the equivalent circuit of the proposed S-shaped MTS-based CP patch antenna were optimized by Advanced Design System (ADS) simulation software. The simulation results were as follows: $L_M = 1.865$ nH, $C_M = 0.85$ pF, $C_G = 0.97$ pF, $L_P = 1.45$ nH, $C_{P1} = 0.775$ pF, $C_{P2} = 0.45$ pF, $L_A = 1.725$ nH, $C_A = 0.93$ pF, and $R_S = 37\ \Omega$.

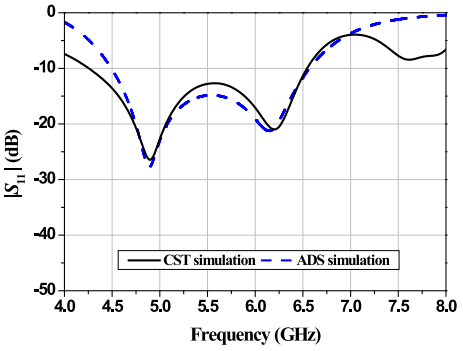

FIGURE 9. Comparison between the CST- and ADS-simulated IBW.

Figure 9 compares the simulated IBW using CST and ADS simulation programs, and the simulation results were in good agreement. Using CST simulation, the lowest resonance frequencies ($|S_{11}| \leq -10$ dB) occurred at 4.87 and 6.22 GHz. Meanwhile, the lowest resonance frequencies ($|S_{11}| \leq -10$ dB) occurred at 4.88 and 6.15 GHz using ADS simulation.

Figures 10 (a)-(b) respectively show the magnified surface current distribution on the S-shaped MTS of the proposed antenna (Antenna III) at 0°, 90°, 180°, and 270° phase at 5.9 GHz and 6.5 GHz. The frequencies of 5.9 GHz and 6.5 GHz corresponded to TM_{10} and TM_{20} resonance modes. The vectors traveled in the +z direction and rotated counterclockwise, giving rise to left-hand circular polarization (LHCP).

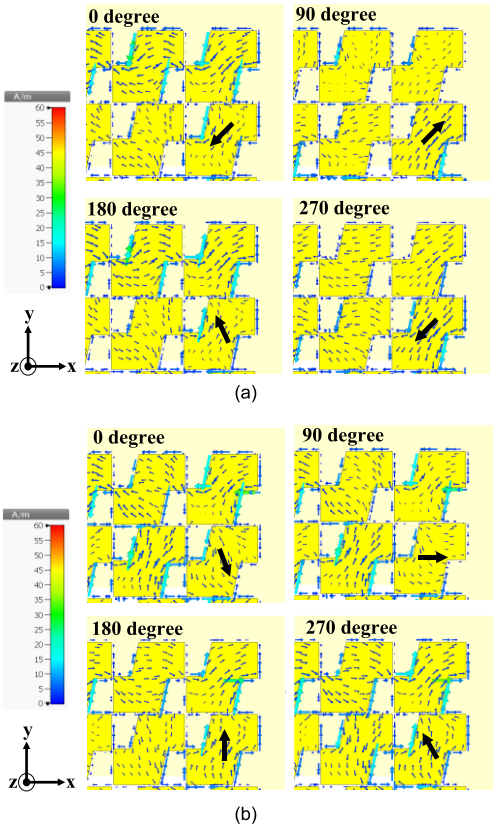

FIGURE 10. Simulated surface current distribution on the S-shaped MTS at 0°, 90°, 180°, and 270° phase: (a) 5.9 GHz, (b) 6.5 GHz.

IV. PARAMETRIC STUDY

This section investigates the effects of key antenna parameters on the IBW and ARBW of the S-shaped MTS-based wideband CP patch antenna. The key antenna parameters included the substrate dimension ($W_{sub} \times L_{sub}$), thickness of the upper substrate (h_3), length of the rectangular-shaped slot (L_s), width of the rectangular-shaped slot (W_s), the length of MTS element (a), and the length of MTS element including voids between two MTS elements (p).

A. EFFECT OF THE SUBSTRATE DIMENSION ($W_{sub} \times L_{sub}$)

Figures 11 (a)-(b) show the simulated IBW ($|S_{11}| \leq -10$ dB) and ARBW (AR ≤ 3 dB) under variable substrate dimensions ($W_{sub} \times L_{sub}$): 30 × 30, 34 × 34, and 38 × 38 mm^2. In Figure 11(a), IBW shifted to lower frequency as the substrate dimension increased. Given the substrate dimensions of 30 × 30 and 38 × 38 mm^2, an impedance mismatch ($|S_{11}| > -10$ dB) occurred over 5.25 – 5.8 GHz and 4.7 – 5.25 GHz, respectively. Similar to IBW, ARBW also shifted to lower frequency with increase in the substrate

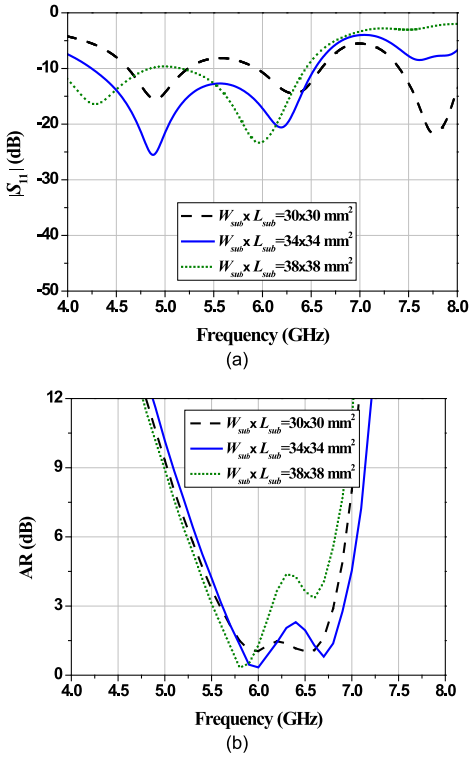

FIGURE 11. Simulated results of the S-shaped MTS CP patch antenna under variable substrate dimensions ($W_{sub} \times L_{sub}$): (a) IBW, (b) ARBW.

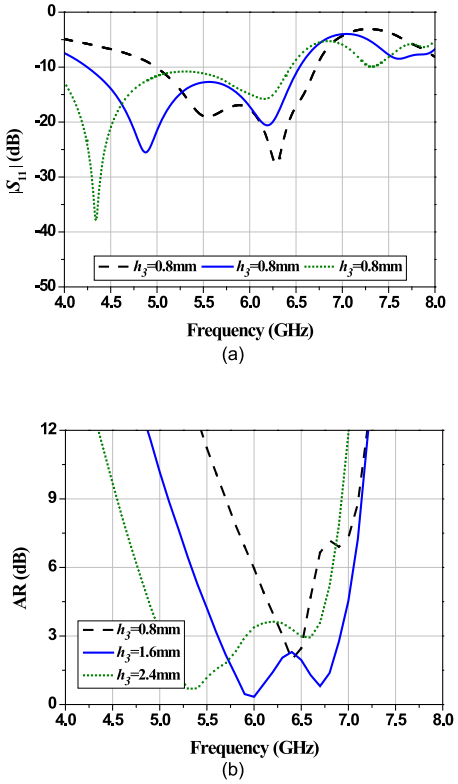

FIGURE 12. Simulated results of the S-shaped MTS CP patch antenna under variable h_3: (a) IBW, (b) ARBW.

dimension, as shown in Figure 11(b). In the figure, ARBW (AR $\leq$ 3 dB) of 30 $\times$ 30 and 38 $\times$ 38 mm^2 substrates were between 5.8 – 6.8 GHz and 5.5 – 6.1 GHz, but with impedance mismatch. With the substrate dimension of 34 $\times$ 34 mm^2, ARBW (5.6 – 6.8 GHz) covered the entire C-band uplink spectrum. As a result, the optimal substrate dimension ($W_{sub} \times L_{sub}$) was 34 $\times$ 34 mm^2.

B. EFFECT OF UPPER SUBSTRATE THICKNESS (h_3)

Figures 12 (a)-(b) show the simulated IBW ($|S_{11}| \leq -10$ dB) and ARBW (AR $\leq$ 3 dB) under variable upper substrate thicknesses (h_3): 0.8, 1.6, and 2.4 mm. In Figure 12(a), as the thickness of the upper substrate increased, IBW was shifting to lower frequency and became wider. Similar to IBW, ARBW also shifted to lower frequency with increase in the upper substrate thickness, as shown in Figure 12(b). Specifically, given $h_3 = 0.8$ mm, ARBW was very narrow (6.3 – 6.5 GHz), seriously falling short of the C-band uplink frequency spectrum (5.925 – 6.425 GHz). With $h_3 = 2.4$ mm, ARBW (5.1 – 5.8 GHz) fell outside the C-band uplink spectrum. With $h_3 = 1.6$ mm, ARBW (5.5 – 6.8 GHz) covered the target C-band spectrum. As a result, the optimal h_3 was 1.6 mm.

C. EFFECT OF THE LENGTH OF RECTANGULAR-SHAPED SLOT (L_s)

Figures 13 (a)-(b) show the simulated IBW and ARBW under different lengths of the rectangular slot on the middle substrate (L_s): 23, 25, and 27 mm. In Figure 13(a), with $L_s = 23$ mm, an impedance mismatch ($|S_{11}| > -10$ dB) occurred between 5.2 – 5.75 GHz. With $L_s = 25$ and 27 mm, IBW fell between 4.2 – 6.5 GHz and 4.2 – 6.45 GHz, respectively, covering the C-band uplink frequency spectrum (5.925 – 6.425 GHz). In Figure 13(b), with $L_s = 23$ and 25 mm, ARBW (AR $\leq$ 3 dB) covered the entire C-band uplink spectrum, with ARBW between 5.6 – 6.85 GHz and 5.5 – 6.8 GHz for $L_s = 23$ and 25 mm, respectively. However, $L_s = 23$ resulted in impedance mismatch. With $L_s = 27$, ARBW was very narrow (5.45 – 6 GHz), failing to cover the entire the C-band uplink spectrum. The optimal L_s was thus 25 mm.

D. EFFECT OF THE WIDTH OF RECTANGULAR-SHAPED SLOT (W_s)

Figures 14 (a)-(b) show the simulated IBW and ARBW under variable widths of the rectangular slot on the middle substrate (W_s): 1.5, 2.0, and 2.5 mm. In Figure 14(a), as Ws increased, $|S_{11}|$ of the first resonance increased (from originally -32.5 dB to -18 dB) while the impedance matching of the second resonance improved. Meanwhile, variation in W_s had a minimal effect on the ARBW of the S-shaped MTS-based CP patch antenna, as shown in Figure 14(b). The optimal W_s was 2.0 mm.

E. EFFECT OF METASURFACE LENGTH (A)

Figures 15 (a)-(b) illustrate the simulated IBW and ARBW under variable MTS lengths (a): 5, 7, and 9 mm. In Figure 15(a), as a increased, the simulated IBW shifted to

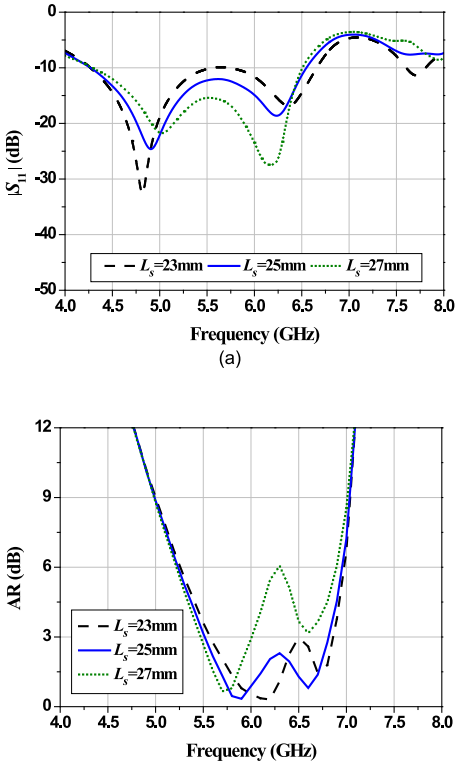

FIGURE 13. Simulated results of the S-shaped MTS CP patch antenna under variable L_S: (a) IBW, (b) ARBW.

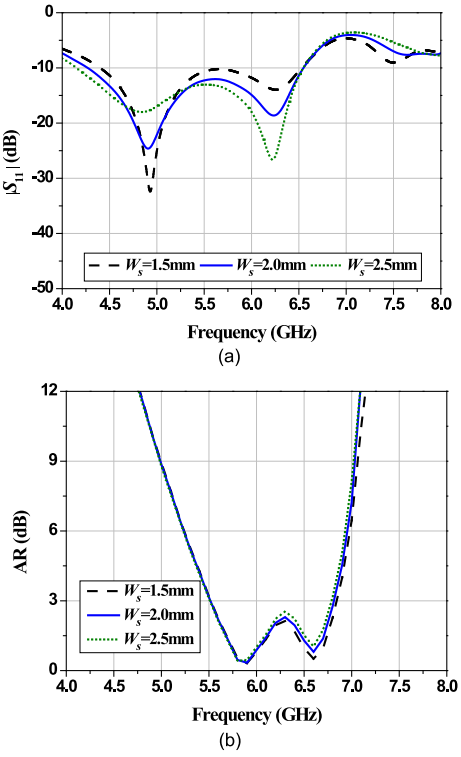

FIGURE 14. Simulated results of the S-shaped MTS CP patch antenna under variable W_S: (a) IBW, (b) ARBW.

lower frequency. However, with excessively large 9 mm, IBW (4.1 – 6.3 GHz) failed to cover the entire C-band uplink

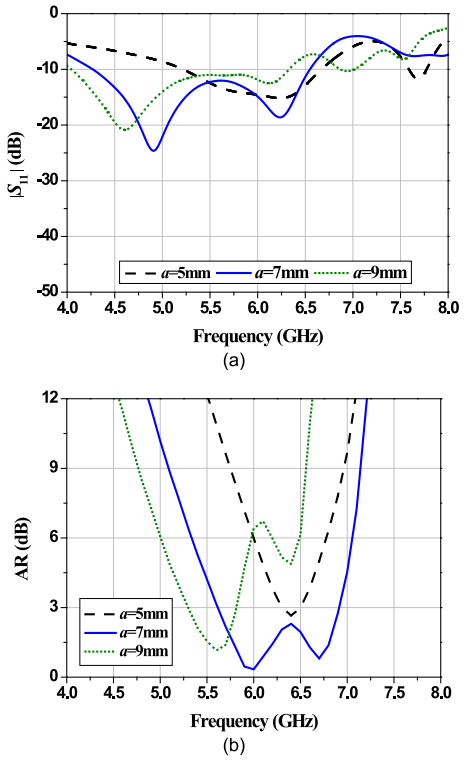

FIGURE 15. Simulated results of the S-shaped MTS CP patch antenna under variable a: (a) IBW, (b) ARBW.

frequency spectrum (5.925 – 6.425 GHz). In Figure 15(b), with $a = 5$ and 9 mm, ARBW (AR $\leq$ 3 dB) were between 6.3 – 6.5 GHz and 5.25 – 5.8 GHz, respectively, failing to cover the entire C-band uplink spectrum. With $a = 7$ mm, ARBW (5.6 – 6.8 GHz) covered the entire C-band uplink spectrum. The optimal a was thus 7 mm.

F. EFFECT OF THE LENGTH OF MTS ELEMENT INCLUDING VOIDS (P)

Figures 16 (a)-(b) show the simulated IBW and ARBW under variable lengths of MTS element including voids (p): 7.2, 7.4, and 7.6 mm. In Figure 16(a), the impedance matching ($|S_{11}|$) significantly improved as p increased, with IBM covering the entire C-band uplink spectrum. In Figure 16(b), with $p = 7.2$ mm, AR was larger than 3 dB (AR $>$ 3 dB) between 5.85 – 6.15 GHz, thus failing to cover the entire C-band uplink spectrum. ARBW were between 5.5 – 6.8 GHz and 5.8 – 6.4 GHz for $p = 7.4$ and 7.6 mm, respectively. By comparison, ARBW of $p = 7.4$ mm was significantly wider than that of $p = 7.6$ mm. The optimal p was thus 7.4 mm.

V. EXPERIMENTAL RESULTS

To validate, a prototype antenna was fabricated and experiments were carried out. Figure 17 depicts the front and rear views of the S-shaped MTS-based CP antenna prototype for the C-band uplink frequency spectrum. The experiments

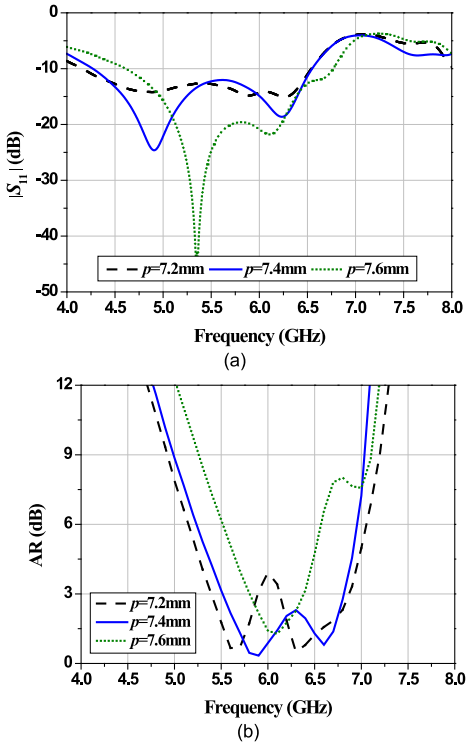

FIGURE 16. Simulated results of the S-shaped MTS CP patch antenna under variable *p*: (a) IBW, (b) ARBW.

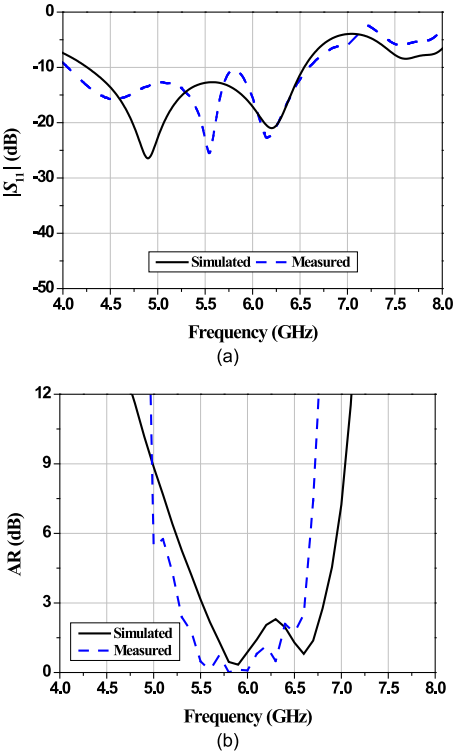

FIGURE 18. The simulated and measured results of the S-shaped MTS-based wideband CP patch antenna: (a) IBW, (b) ARBW.

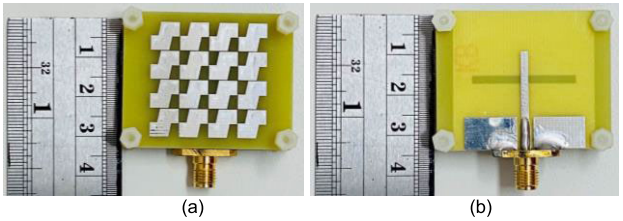

FIGURE 17. A prototype antenna: (a) front view, (b) rear view.

were performed by using a vector network analyzer (ZVB 20 model) in an anechoic chamber.

In Figure 18, the simulated IBW ($|S_{11}| \leq -10$ dB) and ARBW (AR ≤ 3 dB) at the center frequency (5.9 GHz) were 38.98% (4.2 – 6.5 GHz) and 22% (5.5 – 6.8 GHz), and the measured IBW and ARBW were 43.22% (4.05 – 6.6 GHz) and 22% (5.3 – 6.6 GHz). The simulated and measured results were agreeable. The measured ARBW slightly shifted to lower frequency probably due to coaxial connector loss and antenna fabrication. To mount the three substrate layers together, the left and right sides of the substrates of the antenna prototype were each 3 mm wider than the antenna schematic (Figure 1). Nevertheless, the measured ARBW covered the entire C-band uplink frequency spectrum (5.925 – 6.425 GHz).

Figures 19 (a)-(b) compare the simulated and measured LHCP and right-hand circular polarization (RHCP) radiation patterns of the S-shaped MTS-based wideband CP patch antenna in the xz- and yz-planes at 5.9 and 6.5 GHz, respectively. The simulated and measured LHCP were in good agreement, and those of RHCP were satisfactorily agreeable. ETS-Lindgren Model 3100 Series Conical Log Spiral antennas were used to verify the LHCP and RHCP radiations.

Figure 20 illustrates the simulated and measured radiation efficiency and boresight gains of the S-shaped MTS-based wideband CP patch antenna. The simulated and measured results were agreeable, with the measured radiation efficiency over the C-band uplink frequency spectrum was over 70%. The measured 3-dB boresight gain bandwidth was 49.15% (4 – 6.9 GHz), with the maximum gain of 6.16 dBic at 5.6 GHz. The sharp decline in the measured boresight gain beyond 6.5 GHz could be attributed to the low radiation efficiency and impedance mismatch.

Table 2 compares existing MTS-based CP antennas and the proposed low-profile S-shaped MTS-based wideband CP patch antenna in terms of IBW, ARBW, maximum gain, and electrical dimension. In [24], the antenna achieved wide IBW but narrow AR due to the complex design of slanted slot on the ground plane. In [34], the antenna achieved wide IBW and high gain but narrow AR. The antenna design was also very complex as through-holes were drilled between substrates.

In [35], the antenna achieved high gain but suffered from bulkiness and narrow IBW. In [36], the antenna achieved wide IBW and high gain but suffered from bulkiness and failed to cover the C-band uplink frequency spectrum. In [37], the antenna achieved high gain but narrow IBM and AR. The antenna also suffered from bulkiness.

TABLE 2. Comparison between existing MTS-based CP antennas and the proposed low-profile S-shaped MTS-based wideband CP patch antenna.

References	f_0 (GHz)	-10-dB IBW (%)	3-dB ARBW (%)	Maximum gain (dBic)	Electrical dimension
[24]	5.25	33.7	16.5	5.8	$0.60\,\lambda_0 \times 0.49\,\lambda_0 \times 0.070\,\lambda_0$
[34]	5.6	43.5	15.5	7.3	$0.55\,\lambda_0 \times 0.55\,\lambda_0 \times 0.045\,\lambda_0$
[35]	5.8	20.6	17.4	8	$0.79\,\lambda_0 \times 0.79\,\lambda_0 \times 0.067\,\lambda_0$
[36]	5.5	33.6	18.2	7.95	$0.71\,\lambda_0 \times 0.71\,\lambda_0 \times 0.060\,\lambda_0$
[37]	5.5	19	11.7	8.2	$0.79\,\lambda_0 \times 0.79\,\lambda_0 \times 0.067\,\lambda_0$
[38]	5.7	18	12.8	6.9	$0.86\,\lambda_0 \times 0.86\,\lambda_0 \times 0.038\,\lambda_0$
[39]	5.5	18	12.7	12	$1.40\,\lambda_0 \times 1.40\,\lambda_0 \times 0.030\,\lambda_0$
This work	**5.9**	**43.22**	**22**	**6.16**	$\mathbf{0.48\,\lambda_0 \times 0.48\,\lambda_0 \times 0.057\,\lambda_0}$

λ_0: the free-space wavelength corresponding to the lowest operating frequency achievable by the MTS antennas
f_0: the center frequency of the MTS antennas

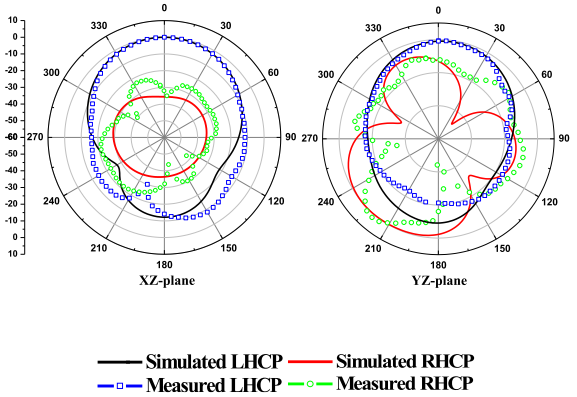

(a)

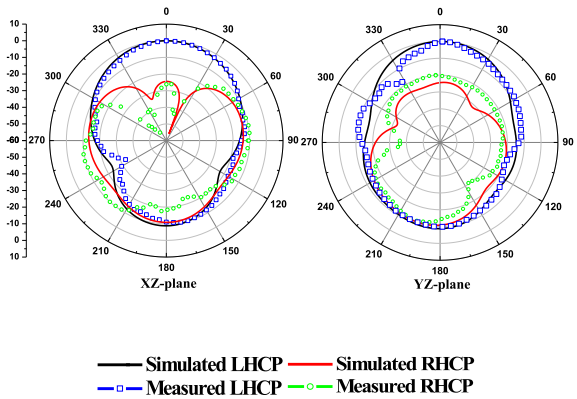

(b)

FIGURE 19. Simulated and measured LHCP (co-polarized) and RHCP (cross-polarized) radiation patterns at: (a) 5.9 GHz, (b) 6.5 GHz.

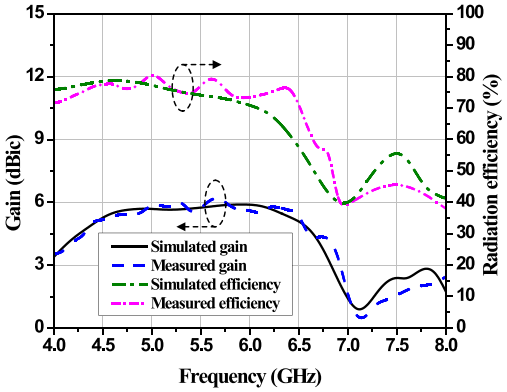

FIGURE 20. Simulated and measured radiation efficiency and boresight gains of the proposed antenna.

In [38], the single-layer MTS antenna had a straightforward design but suffered from narrow IBM, AR, and bulkiness. In [39], the sequential-phase fed CP patch array, consisting of a single-layer substrate and 2 × 2 patch array, achieved high gain but suffered from the sequential-phase design complexity and bulkiness.

For antennas operable in the C-band frequency spectrum (4 – 8 GHz), the proposed low-profile S-shaped MTS-based wideband CP patch antenna efficiently achieved wide IBW and ARBW. Specifically, the proposed MTS-based CP patch antenna is the deployment of S-shaped MTS elements to efficiently convert linear polarization (LP) into circular polarization (CP) waves for the C-band uplink frequency spectrum. The proposed antenna achieves wide IBW and ARBW of 43.22% (4.05 - 6.6 GHz) and 22% (5.3 – 6.6 GHz) with low-profile structure, rendering the antenna scheme suitable for satellite communication applications.

VI. CONCLUSION

This research proposed a low-profile S-shaped MTS-based wideband CP patch antenna for C-band uplink frequency spectrum. The proposed antenna was fabricated on three layers of FR-4 substrate: upper, middle, and lower, without air gap between substrates. The upper substrate contained 4 × 4 periodic S-shaped MTS elements, the middle substrate functioned as the ground plane with a rectangular-shaped slot at the center, and the lower substrate consisted of CPW. In the operation, the coupling between the rectangular-shaped slot and the CPW generated LP wave which was converted into CP wave by the S-shaped MTS elements. Simulations were carried out, and an antenna prototype was fabricated and experiments carried out. The simulated IBW ($|S_{11}| \leq -10$ dB) and ARBW (AR $\leq$ 3 dB) at the center frequency

of 5.9 GHz were 38.98% (4.2 – 6.5 GHz) and 22% (5.5 – 6.8 GHz), and the measured IBW and ARBW were 43.22% (4.05 – 6.6 GHz) and 22% (5.3 – 6.6 GHz). The simulated and measured LHCP radiation patterns were in good agreement, with the measured maximum gain of 6.16 dBic at 5.6 GHz. Given the IBW and ARBW of 43.22% (4.05 – 6.6 GHz) and 22% (5.3 – 6.6 GHz), the proposed S-shaped MTS-based wideband CP patch antenna is suitable for satellite communication applications.

REFERENCES

[1] H. Nasimuddin, X. Qing, and Z. N. Chen, "A compact circularly polarized slotted patch antenna for GNSS applications," *IEEE Trans. Antennas Propag.*, vol. 62, no. 12, pp. 6506–6509, Dec. 2014.

[2] R. Cao and S.-C. Yu, "Wideband compact CPW-fed circularly polarized antenna for universal UHF RFID reader," *IEEE Trans. Antennas Propag.*, vol. 63, no. 9, pp. 4148–4151, Sep. 2015.

[3] K. W. Lui, O. H. Murphy, and C. Toumazou, "A wearable wideband circularly polarized textile antenna for effective power transmission on a wirelessly-powered sensor platform," *IEEE Trans. Antennas Propag.*, vol. 61, no. 7, pp. 3873–3876, Jul. 2013.

[4] S. K. K. Dash, T. Khan, and B. K. Kanaujia, "Circularly polarized dual facet spiral fed compact triangular dielectric resonator antenna for sensing applications," *IEEE Sensors Lett.*, vol. 2, no. 1, Mar. 2018, Art. no. 3500404.

[5] B. Bahreini, H. Oraizi, N. Noori, and S. Fakhte, "Design of a circularly polarized parasitic array with slot-coupled DRA with improved gain for the 5G mobile system," *IEEE Antennas Wireless Propag. Lett.*, vol. 17, no. 10, pp. 1802–1806, Oct. 2018.

[6] J.-H. Bang, C. Bat-Ochir, H.-S. Koh, E.-J. Cha, and B.-C. Ahn, "A small and lightweight antenna for handheld RFID reader applications," *IEEE Antennas Wireless Propag. Lett.*, vol. 11, pp. 1076–1079, Sep. 2012.

[7] K.-L. Wong, F.-R. Hsiao, and C.-L. Tang, "A low-profile omnidirectional circularly polarized antenna for WLAN access point," in *Proc. IEEE Antennas Propag. Soc. Symp.*, Monterey, CA, USA, 2004, pp. 2580–2583.

[8] K.-B. Ng, C. H. Chan, and K.-M. Luk, "Low-cost vertical patch antenna with wide axial-ratio beamwidth for handheld satellite communications terminals," *IEEE Trans. Antennas Propag.*, vol. 63, no. 4, pp. 1417–1424, Apr. 2015.

[9] S. Gao, Q. Luo, F. Zhu, *Circularly Polarized Antennas*. Hoboken, NJ, USA: Wiley, 2014.

[10] N. Supreeyatitikul, N. Teerasuttakorn, P. Boontamchauy, and M. Rattanasuttikan, "A compact printed wideband circularly polarized slot antenna for universal UHF RFID reader," in *Proc. 14th Eur. Conf. Antennas Propag. (EuCAP)*, Copenhagen, Denmark, Mar. 2020, pp. 1–5.

[11] X. M. Qing and Y. W. M. Chia, "Broadband circularly polarised slot loop antenna fed by three-stub hybrid coupler," *Electron. Lett.*, vol. 35, no. 15, pp. 1210–1211, Jul. 1999.

[12] H. Yang, Y. Fan, and X. Liu, "A compact dual-band stacked patch antenna with dual circular polarizations for BeiDou navigation satellite systems," *IEEE Antennas Wireless Propag. Lett.*, vol. 18, no. 7, pp. 1472–1476, Jul. 2019.

[13] G. Feng, L. Chen, X. Wang, X. Xue, and X. Shi, "Broadband circularly polarized crossed bowtie dipole antenna loaded with parasitic elements," *IEEE Antennas Wireless Propag. Lett.*, vol. 17, no. 1, pp. 114–117, Jan. 2018.

[14] R. Chair, S. L. S. Yang, A. A. Kishk, K. F. Lee, and K. M. Luk, "Aperture fed wideband circularly polarized rectangular stair shaped dielectric resonator antenna," *IEEE Trans. Antennas Propag.*, vol. 54, no. 4, pp. 1350–1352, Apr. 2006.

[15] N. Nasimuddin, Z. N. Chen, and X. Qing, "Bandwidth enhancement of a single-feed circularly polarized antenna using a metasurface: Metamaterial-based wideband CP rectangular microstrip antenna," *IEEE Antennas Propag. Mag.*, vol. 58, no. 2, pp. 39–46, Apr. 2016.

[16] S. X. Ta, T. H. Nguyen, K. K. Nguyen, and C. Dao-Ngoc, "Bandwidth-enhancement of circularly-polarized Fabry–Perot antenna using single-layer partially reflective surface," *Int. J. RF Microw. Comput.-Aided Eng.*, vol. 29, no. 8, Aug. 2019, Art. no. e21774.

[17] S. X. Ta, I. Park, and R. W. Ziolkowski, "Crossed dipole antennas: A review," *IEEE Antennas Propag. Mag.*, vol. 57, no. 5, pp. 107–122, Oct. 2015.

[18] K. Srivastava, A. Kumar, P. Chaudhary, B. K. Kanaujia, S. Dwari, A. K. Verma, K. P. Esselle, and R. Mittra, "Wideband and high–gain circularly polarised microstrip antenna design using sandwiched metasurfaces and partially reflecting surface," *IET Microw., Antennas Propag.*, vol. 13, no. 3, pp. 305–312, Feb. 2019.

[19] X. Li, M. Memarian, and T. Itoh, "A new cavity resonance assisted by anisotropic metasurfaces," *IEEE Trans. Microw. Theory Techn.*, vol. 66, no. 7, pp. 3224–3233, Jul. 2018.

[20] S. X. Ta and I. Park, "Low-profile broadband circularly polarized patch antenna using metasurface," *IEEE Trans. Antennas Propag.*, vol. 63, no. 12, pp. 5929–5934, Dec. 2015.

[21] N. Hussain, M.-J. Jeong, A. Abbas, T.-J. Kim, and N. Kim, "A metasurface-based low-profile wideband circularly polarized patch antenna for 5G millimeter-wave systems," *IEEE Access*, vol. 8, pp. 22127–22135, 2020.

[22] T. Yue, Z. H. Jiang, and D. H. Werner, "Compact, wideband antennas enabled by interdigitated capacitor-loaded metasurfaces," *IEEE Trans. Antennas Propag.*, vol. 64, no. 5, pp. 1595–1606, May 2016.

[23] M. Faenzi, G. Minatti, D. González-Ovejero, F. Caminita, E. Martini, C. Della Giovampaola, and S. Maci, "Metasurface antennas: New models, applications and realizations," *Sci. Rep.*, vol. 9, no. 1, Dec. 2019, Art. no. 10178.

[24] Z. Wu, L. Li, Y. Li, and X. Chen, "Metasurface superstrate antenna with wideband circular polarization for satellite communication application," *IEEE Antennas Wireless Propag. Lett.*, vol. 15, pp. 374–377, Jun. 2016.

[25] C. A. Balanis, *Antenna Theory: Analysis and Design*, 3rd ed. Hoboken, NJ, USA: Wiley, 2005.

[26] W. Liu, Z. N. Chen, and X. Qing, "Metamaterial-based low-profile broadband mushroom antenna," *IEEE Trans. Antennas Propag.*, vol. 62, no. 3, pp. 1165–1172, Mar. 2014.

[27] H. Kang and S.-O. Park, "Mushroom meta-material based substrate integrated waveguide cavity backed slot antenna with broadband and reduced back radiation," *IET Microw., Antennas Propag.*, vol. 10, pp. 1598–1603, Nov. 2016.

[28] W. E. I. Liu, Z. N. Chen, X. Qing, J. Shi, and F. H. Lin, "Miniaturized wideband metasurface antennas," *IEEE Trans. Antennas Propag.*, vol. 65, no. 12, pp. 7345–7349, Dec. 2017.

[29] H. L. Zhu, S. W. Cheung, K. L. Chung, and T. I. Yuk, "Linear-to-circular polarization conversion using metasurface," *IEEE Trans. Antennas Propag.*, vol. 61, no. 9, pp. 4615–4623, Sep. 2013.

[30] M. Ameen and R. K. Chaudhary, "Dual-layer and dual-polarized metamaterial inspired antenna using circular-complementary split ring resonator mushroom and metasurface for wireless applications," *Int. J. Electron. Commun.*, vol. 113, pp. 1–18, Jan. 2020.

[31] M. Ameen, A. Mishra, and R. K. Chaudhary, "Asymmetric CPW-fed electrically small metamaterial-inspired wideband antenna for 3.3/3.5/5.5 GHz WiMAX and 5.2/5.8 GHz WLAN applications," *Int. J. Electron. Commun.*, vol. 119, pp. 1–11, May 2020.

[32] N. Mishra, A. Gupta, and R. K. Chaudhary, "A compact CPW-fed wideband metamaterial antenna using Ω-shaped interdigital capacitor for mobile applications," *Microw. Opt. Technol. Lett.*, vol. 57, no. 11, pp. 2558–2562, Nov. 2015.

[33] A. Gupta and R. K. Chaudhary, "The metamaterial antenna: A novel miniaturized dual-band coplanar waveguide-fed antenna with backed ground plane," *IEEE Antennas Propag. Mag.*, vol. 60, no. 4, pp. 41–48, Aug. 2018.

[34] X.-M. Xu and C.-W. Huang, "Wideband and low profile polarization conversion metasurface-based circularly polarized slot antenna," *Int. J. RF Microw. Comput.-Aided Eng.*, vol. 29., no. 5, e21662, May 2019.

[35] Q. Zheng, C. Guo, and J. Ding, "Wideband and low RCS circularly polarized slot antenna based on polarization conversion of metasurface for satellite communication application," *Microw. Opt. Technol. Lett.*, vol. 60, no. 3, pp. 679–685, Mar. 2018.

[36] L. Yuan, H. Yu-Xuan, L. Zhan-Wei, C. Shu-Ting, X. Xiao-Ming, and G. Jing, "Design of a compact wideband CP metasurface antenna," *Int. J. RF Microw. Comput.-Aided Eng.*, vol. 30, no. 10, Oct. 2020, Art. no. e22332.

[37] Y. Liu, Y.-X. Huang, Z.-W. Liu, S.-T. Cai, X.-M. Xiong, and J. Guo, "A new broadband circularly polarized antenna with a single-layer metasurface," *Int. J. RF Microw. Comput. Aided Eng.*, vol. 30, no. 7, Jul. 2020, Art. no. e22226.

[38] Z. Liang, J. Ouyang, and F. Yang, "Low-profile wideband circularly polarised single-layer metasurface antenna," *Electron. Lett.*, vol. 54, no. 24, pp. 1362–1364, Nov. 2018.
[39] C. Deng, Y. Li, Z. Zhang, and Z. Feng, "A wideband sequential-phase fed circularly polarized patch array," *IEEE Trans. Antennas Propag.*, vol. 62, no. 7, pp. 3890–3893, Jul. 2014.

NATHAPAT SUPREEYATITIKUL was born in Nakhon Si Thammarat, Thailand, in 1991. He received the B.Eng. degree from Mahidol University, Thailand, in 2014, and the M.Eng. degree from the King Mongkut's University of Technology Thonburi (KMUTT), Thailand, in 2016. He is currently pursuing the D.Eng. degree with the King Mongkut's Institute of Technology Ladkrabang (KMITL). His research interests include circularly polarized antennas and MIMO antennas.

TITIPONG LERTWIRIYAPRAPA (Senior Member, IEEE) received the B.S.Tech.Ed. degree in electrical engineering from the King Mongkut's University of Technology North Bangkok, in 1996, the M.Eng. degree in electrical engineering from the King Mongkut's Institute of Technology Ladkrabang, in 2000, and the M.Sc. and Ph.D. degrees in electrical engineering from The Ohio State University, Columbus, OH, USA, in 2006 and 2007, respectively. He is currently an Associate Professor with the Department of Teacher Training in Electrical Engineering, King Mongkut's University of Technology, North Bangkok. His research interests include electromagnetic theory, metamaterial, asymptotic, computational electromagnetics, and hybrid methods. He received the third place in the 2007 USNC/CNC URSI Student Paper Competition, held in Ottawa, Canada, and the Best Paper Award from the 2008 International Symposium on Antennas and Propagation (ISAP2008), Taiwan. He was with the Board Committee of the ECTI Association, from 2012 to 2015.

CHUWONG PHONGCHAROENPANICH (Member, IEEE) received the B.Eng. (Hons.) degree in telecommunications engineering and the M.Eng. and D.Eng. degrees in electrical engineering from the King Mongkut's Institute of Technology Ladkrabang (KMITL), Bangkok, Thailand, in 1996, 1998, and 2001, respectively. He is currently an Associate Professor with the Department of Telecommunications Engineering, KMITL, where he also serves as the Leader of the Innovative Antenna and Electromagnetic Applications Research Laboratory. His research interests include antenna design for various mobile and wireless communications, array antennas, electromagnetic theory and applications. He is also a member of IEICE and ECTI. He has served as the Chair of the IEEE MTT/AP/ED Thailand Chapter, from 2014 to 2018. He has been on organizing committee of several international conferences, including the TPC Chair of 2009 International Symposium on Antennas and Propagation (ISAP 2009), TPC member of ISAP 2012, and a Vice Chair of ISAP 2017. He is also a Reviewer of many scientific journals, including the IEEE TRANSACTIONS ON ANTENNAS AND PROPAGATION, IEEE ACCESS, *IET Microwaves, Antennas and Propagation*, *Electronics Letters*, and *ECTI Transactions*, and many international conferences, including ISAP and APMC. He was on the Board Committee of ECTI Association, from 2008 to 2011 and from 2014 to 2015. He was an Associate Editor of the *IEICE Transactions on Communications* and the *ECTI Transactions on Electrical Engineering, Electronics, and Communications*. He is also an Associate Editor of the *IEICE Communications Express*.